Int J Adv Manuf Technol (2008) 39:9–20
DOI 10.1007/s00170-007-1193-7

ORIGINAL ARTICLE

Design of horn for rotary ultrasonic machining using the finite element method

Vinod Yadava · Aniruddha Deoghare

Received: 3 March 2007 / Accepted: 27 July 2007 / Published online: 9 September 2007

Abstract The cutting performance of an ultrasonic machining machine (USM) depends primarily on the ability of the design of the acoustic horn (also known as concentrator or tool holder). A horn is a waveguide-focusing device with a cross-sectional area that decreases from the transducer end to the toe end. It amplifies the input amplitude of vibrations so that at the output end the amplitude is sufficiently large for machining. In the present work, a finite element method (FEM) design procedure has been developed for the design of a horn for rotary ultrasonic machining (RUM). The double conical horn shape has taken as a domain with a hole at the tip for the cooling purpose. The analysis of the various stress components in the horn domain has been studied. The stresses at the middle of the horn are found to be maximum but it is within the allowable stress of the horn material due to the sudden change in the area of the horn. The stresses on the horn for various frequencies are also studied and concluded that at resonance condition the stress is minimum.

Keywords Rotary ultrasonic machining (RUM) · Horn · Stresses · Finite element method (FEM)

1 Introduction

With the development of technology, more and more challenging problems are faced by the engineers and technologists in the field of manufacturing. Recently, many new engineering materials have been developed, many of which are very difficult to machine. This applies particularly to super-hard materials, such as tungsten and titanium carbides, diamonds, hard steels, magnetic alloys and corundum. Grinding is the only technique used for machining these materials [1]. Another group of materials, like germanium, silicon, ferrite, ceramics, glass, and quartz gives difficulty in machining on account of their higher brittleness. These materials often not able to withstand the forces needed for shaping [1]. The complex shapes in these materials are either difficult to machine or time-consuming by the traditional processes. The need for methods of shaping these unshapable materials with the requirements of higher production rate at cheaper rates may demand the use of non-traditional processes [1].

The various unconventional machining processes commonly used are electro discharge machining (EDM), laser beam machining (LBM), electron beam machining (EBM), plasma beam machining (PBM), ion beam machining (IBM), chemical machining (CHM), bio-chemical machining (BCHM), electro chemical machining (ECM), ultrasonic machining (USM), abrasive and/or water jet machining (A/WJM), etc. Ultrasonic machining (USM) is a unconventional mechanical-type material-removal process generally associated with low material removal rates, however, its application is not limited by the electrical or chemical characteristics of the workpiece materials. It is used for both conductive and non-conductive materials. Holes as small as 76 μm in diameter can be machined, however, the depth to diameter ratio is limited to about 3:1.

USM is used for machining hard and brittle materials to complex shapes with good accuracy and reasonable surface finish. This process is not affected by the electrical or chemical characteristics of the work material. Holes of any shape can be produced and it has no high-speed moving

V. Yadava (✉) · A. Deoghare
Department of Mechanical Engineering,
Motilal Nehru National Institute of Technology,
Allahabad 211004, India
e-mail: vinody@mnnit.ac.in

parts. Working is not hazardous. Power consumption is about 0.1-Watt hour/mm^3 for glass and about 5.0-Watt hour/mm^3. However, in USM, the slurry has to be fed to and removed from the gap between the tool and the workpiece. Because of this fact, there are some disadvantages of this method. The material removal rate slows down considerably and even stops as penetration depth increases. The slurry may wear the wall of the machined hole as it passes back towards the surface, which limits the accuracy, particularly for small holes. The ultrasonic method is based on abrasion phenomenon. The brittle material is removed by blows from grains of a harder abrasive, which is under the control of a tool that vibrates with comparatively small amplitude [2, 3].

Rotary ultrasonic machining (RUM) was invented by Legge in 1964. In the first rotary ultrasonic machining device, the slurry was abandoned and a vibrating diamond-impregnated tool was used against a rotating workpiece. Because the workpieces were held in a rotating four-jaw chuck, with this device only circular holes could be machined and only comparatively small workpieces could be drilled. Further improvements led to the development of a machine comprising a rotating ultrasonic transducer [4]. The rotating transducer head made it possible to precisely machine stationary workpieces to close tolerances.

For a long time, rotary ultrasonic machining was viewed merely as an improvement of USM. One of the major difference between USM and RUM is that USM uses a soft tool (such as stainless steel, brass, and mild steel) and slurry loaded with hard abrasive particles while in RUM the hard abrasive particles (diamond) are bonded on the tools. Rotary ultrasonic machining is performed by a cutting tool that vibrates at constant high frequency (typically 20 kHz). An abrasive slurry or suspension is fed into the space between the workpiece and the longitudinally vibrating tool. Under the action of the constant reciprocating force applied to the tool, the abrasive particles in the slurry remove material from the workpiece in the form of minute particles. As material is removed, a cavity is formed in the workpiece. This high-speed reciprocation of the tool drives the abrasive grains across a small gap against the workpiece. The impact of the abrasives is principally responsible for material removal.

Figure 1 shows a schematic diagram of a rotary ultrasonic machine setup. The resonance transducer or vibrator acts as the source of mechanical oscillations, transforming the electrical power received from the generator into mechanical vibration. However, the amplitude of the resulting ultrasonic vibrations is inadequate for realization of the cutting process. To overcome this inadequacy, a wave-guide focusing device known as a horn (also known as concentrator or tool holder), is fitted onto the end of the transducer. This horn has a cross sectional area that

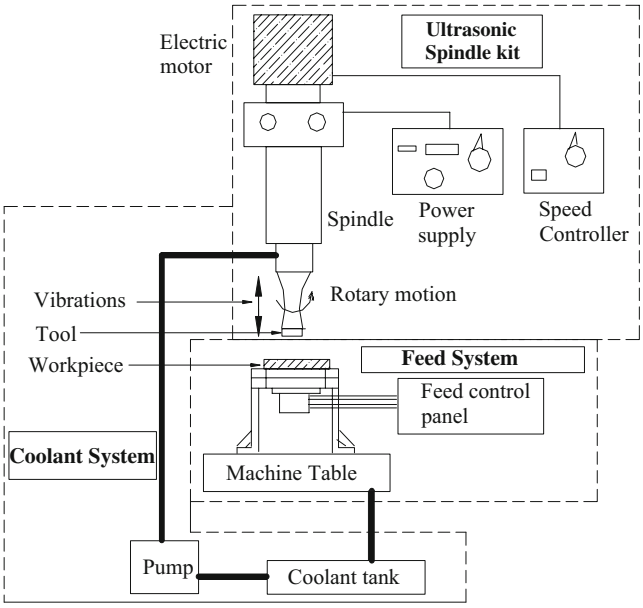

Fig. 1 A set-up of rotary USM

decreases from the input (transducer) end to the output (tool) end. It therefore amplifies the input amplitude of vibration so that at the output end the amplitude is sufficiently large for machining. The tool attached to the end of the horn makes it possible to form a hole in the workpiece [5]. The vibratory system formed by the transducer, horn, and tool is mounted securely on a stand by means of a special clamping system. The basic elements of ultrasonic machine tool comprises of the (i) ultrasonic generator and transducer (ii) ultrasonic horn and tool assembly (iii) tool feed mechanism (iv) abrasive slurry feed system.

In rotary USM, an additional motion is given to the horn in addition to the usual parameters that exist in conventional USM. The rotation of the horn causes new situations of cutting to develop in the machining zone. Sliding/rolling contact would exist between abrasive grains and the workpiece being machined. The sliding/rolling contact causes a higher material removal rate and hence the machining time is reduced considerably in rotary USM as compared to that of conventional USM. In rotary USM, as the speed of rotation of the horn is increased, the penetration rate increases. The superior performance of rotary USM over conventional USM may be explained by the combined effects of indentation of the workpiece surface, sliding contact between the embedded grains on the workpiece, and the rolling contact between the free abrasive grains and the workpiece.

Amin et al. [6] have studied the design of horns for conventional ultrasonic machining process by employing finite element method. They suggested that the horn profile should be conical at the upper end and cylindrical at the

lower end. Seah et al. [7] have obtained the frequencies for the three methods of simulation in the modal analysis, and compared with the experimentally measured frequency. They also suggested that the conical horns should not fail by fatigue or by yielding since the stresses encountered are fairly low. Komaraiah and Reddy [8, 9] shows the superior performance of rotary ultrasonic machining over conventional ultrasonic machining. They demonstrate in rotary ultrasonic machining that there must be rolling contact between the workpiece and the abrasives particles. They also suggested that in rotary USM, as the speed of the rotation increases, the penetration rate increases. Pei et al. [10] proposed a new approach to extend rotary ultrasonic machining to face milling of ceramics. They suggested the various assumptions for rotary ultrasonic machining process. Thoe et al. [11] shows the superior performance of rotary USM over conventional USM and explained by the combined effects of indentation of the workpiece surface, sliding contact between the embedded grains and the workpiece and rolling contacts between the free abrasive grains and workpiece.

From the above literature survey it can be observed that the analysis of horn for conventional USM without horn rotation has been done. People worked experimentally and theoretically for finding the material removal rate using conventional USM and rotary USM, but the theoretical model for the design of horn for rotary USM has not been yet done. In the present work, the goal is to design the horn for ultrasonic machining with rotation within the working condition of ultrasonic machining. In the present analysis, FEM-based model is developed to calculate the resonance frequency, the axial amplitude, and the stress components over the horn domain for the USM with rotation.

2 Mathematical modeling

A rigorous solution to the problem of the propagation of the low-amplitude vibrations in a rod of finite length with reducing cross section presents mathematical difficulties [7]. Hence, several simplifying assumptions are made for technical calculations to make the problem mathematically tractable.

1. A plane wave is propagated in the rod, that is, the stresses and the velocities of the particles over the whole area of a cross section are constant.
2. The transverse compression of the rod is neglected, as it is not taking part in the cutting operation.
3. The slurry acts as a coolant for the horn, tool, and workpiece, supplies fresh abrasives to the cutting zone and removes debris from the cutting area.
4. The material for the horn is homogeneous and isotropic. There is no change in the material properties of horn along the length of the horn.

2.1 Governing equations

The equation of equilibrium for stresses in an axisymmetric rod are given as [12–14]

$$\begin{aligned} \frac{\partial \sigma_{rr}}{\partial r} + \frac{\partial \sigma_{rz}}{\partial z} + \frac{\sigma_{rr} - \sigma_{\theta\theta}}{r} + b_r = 0 \\ \frac{\partial \sigma_{rz}}{\partial r} + \frac{\partial \sigma_{zz}}{\partial z} + \frac{\sigma_{rz}}{r} + b_z = 0 \end{aligned} \tag{1}$$

where σ_{rr}, σ_{zz} and $\sigma_{\theta\theta}$ are the normal stresses in the r, z and θ direction σ_{rz} is the shear stress in rz plane, b_r, b_z are body forces in the r and z direction.

The stress distribution in the rotating circular disks is of great practical importance. If the thickness of the disk is small in comparison to its radius, the variation of the radial and tangential stresses over the thickness can be neglected. If the thickness of the disk is greater than its radius, it is necessary to put the body force equal to the rotary inertia force [12–14]. Then,

$$b_r = \rho n^2 r \quad \text{and} \quad b_z = 0$$

where ρ is the mass per unit volume of the material of the disk and n is the revolution per minute of the disk.

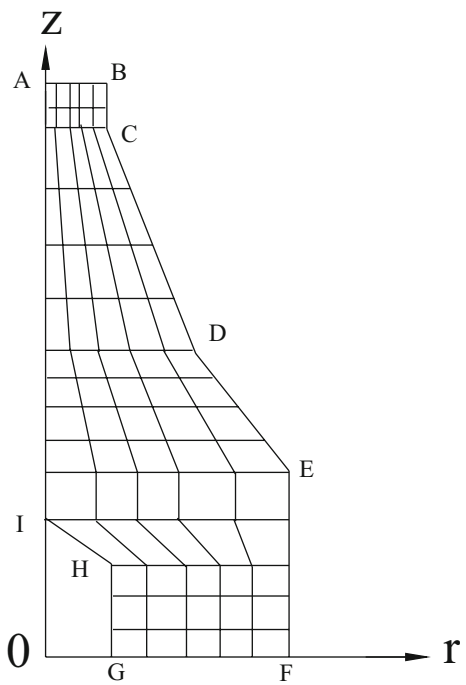

Fig. 2 Schematic of horn of rotary ultrasonic machining with finite element mesh

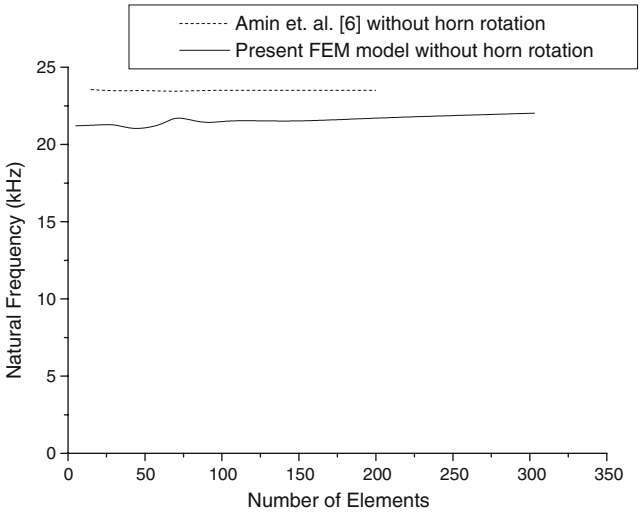

Fig. 3 Effect of number of elements on the natural frequency

So Eq. (1) in the present case becomes,

$$\frac{\partial \sigma_{rr}}{\partial r}+\frac{\partial \sigma_{rz}}{\partial z}+\frac{\sigma_{rr}-\sigma_{\theta\theta}}{r}+\rho n^2 r=0$$
$$\frac{\partial \sigma_{rz}}{\partial r}+\frac{\partial \sigma_{zz}}{\partial z}+\frac{\sigma_{rz}}{r}=0 \qquad (2)$$

Due to the vibration of the rod, the longitudinal extension and compression takes place [15–17]. Hence Eq. (2) becomes

$$\frac{\partial \sigma_{rr}}{\partial r}+\frac{\partial \sigma_{rz}}{\partial z}+\frac{\sigma_{rr}-\sigma_{\theta\theta}}{r}+\rho n^2 r=\rho\frac{\partial^2 u_r}{\partial t^2}$$
$$\frac{\partial \sigma_{rz}}{\partial r}+\frac{\partial \sigma_{zz}}{\partial z}+\frac{\sigma_{rz}}{r}=\rho\frac{\partial^2 u_z}{\partial t^2} \qquad (3)$$

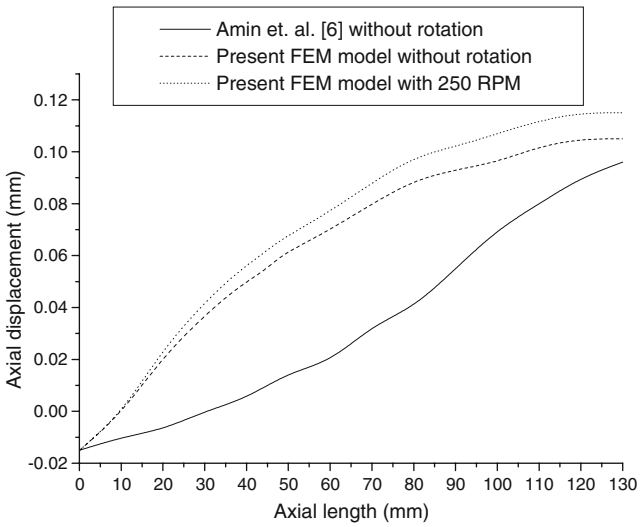

Fig. 4 Variation of axial displacement along the axial length of a double conical horn at the resonance condition

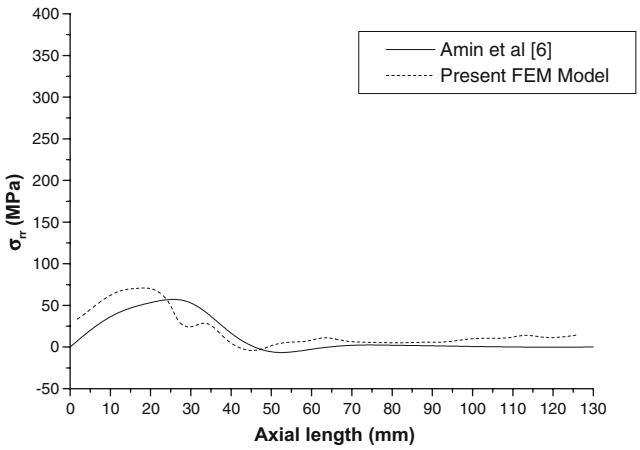

Fig. 5 Variation of radial stress (σ_{rr}) along the axial length

where $\rho\frac{\partial^2 u_r}{\partial t^2}$ is the inertia force in the r direction and $\rho\frac{\partial^2 u_z}{\partial t^2}$ is the inertia force in the z direction.

So Eq. (3) becomes the governing equation for the rotating horn of any shape (such as exponential, conical or stepped). After application of boundary conditions, resonance length of the horn can be calculated so that good amplitude can be obtained, which is necessary for the cutting purpose.

2.2 Boundary conditions

As the horn for rotary USM is given the initial amplitude at the transducer end [6], the essential boundary condition (EBC) becomes

$$u_r=u_r^* \qquad \text{on GF}$$
$$u_z=u_z^*$$

where u_r^* is the displacement along the radial (transverse) direction and is equal to 0 and u_z^* is the displacement along

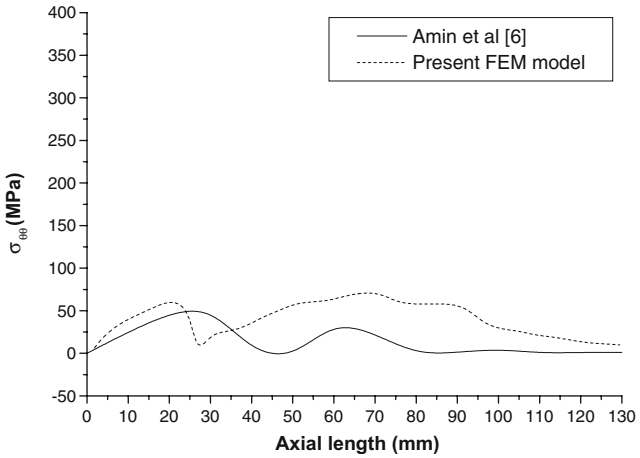

Fig. 6 Variation of circumferential stress ($\sigma_{\theta\theta}$) along the axial length

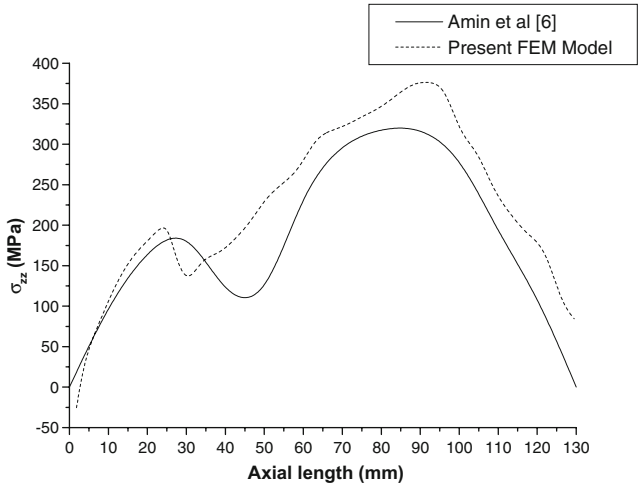

Fig. 7 Variation of axial stress (σ_{zz}) along the axial length

the axial (longitudinal) direction and equal to 15 μm in transducer end GF at every node as shown in Fig. 2 and the natural boundary conditions (NBC) are

$$\begin{aligned} \sigma_{rr}n_r + \sigma_{rz}n_z &= t_r \\ \sigma_{rz}n_r + \sigma_{zz}n_z &= t_z \end{aligned} \quad \text{on} \quad \text{GHIABCDEF} \qquad (4)$$

where σ_{rr} is the normal stress in the radial direction σ_{rz} is the shear stress in the rz plane t_r and t_z are the traction forces in the radial and axial direction, respectively, n_r and n_z are the unit vectors in the radial and axial direction, respectively.

3 Finite element formulation

In the generation of elemental equation, the bilinear and linear form of the equation are written in matrix form related to nodal values as, bilinear form of equation in matrix form

$$\left([K]^e - \omega^2[M]^e\right)\{u\}^e = \{f_b\}^e + \{f_t\}^e \qquad (5)$$

Table 1 Specifications of horn for rotary ultrasonic machining using the finite element method

Parameters	
Modulus of elasticity, E Steel AISI (4063)	200 GPA
Poisson's ratio í Steel AISI (4063)	0.33
Mass density ñ Steel AISI (4063)	7,800 kg/m^3
Endurance strength σ_e Steel AISI (4063)	733 MPa
The allowable endurance limit of Steel AISI (4063)	520 MPa
Resonance frequency	20–25 kHz
Transducer amplitude	15 μm
Transducer diameter	40 mm
Tool diameter	10 mm
Length of horn	130 mm
RPM, n	250

where,

$$[K]^e = \text{Elemental Stiffness matrix} = \int_D [B]^{eT}[D][B]^e r dr dz$$

$[B]^e$ is the derivative of shape function matrix

$$[B]^e = \begin{bmatrix} \frac{\partial N_1}{\partial r} & 0 & \frac{\partial N_2}{\partial r} & 0 & \cdots & \frac{\partial N_{nne}}{\partial r} & 0 \\ \frac{N_1}{r} & 0 & \frac{N_2}{r} & 0 & \cdots & \frac{N_{nne}}{r} & 0 \\ 0 & \frac{\partial N_1}{\partial z} & 0 & \frac{\partial N_2}{\partial z} & \cdots & 0 & \frac{\partial N_{nne}}{\partial z} \\ \frac{\partial N_1}{\partial z} & \frac{\partial N_1}{\partial r} & \frac{\partial N_2}{\partial z} & \frac{\partial N_2}{\partial r} & \cdots & \frac{\partial N_{nne}}{\partial z} & \frac{\partial N_{nne}}{\partial r} \end{bmatrix}$$

$[D]$ is the matrix of elastic constant

$$[D] = \frac{E}{(1+\upsilon)(1-2\upsilon)} \begin{bmatrix} 1-\upsilon & \upsilon & \upsilon & 0 \\ \upsilon & 1-\upsilon & \upsilon & 0 \\ \upsilon & \upsilon & 1-\upsilon & 0 \\ 0 & 0 & 0 & \frac{1-2\upsilon}{2} \end{bmatrix}$$

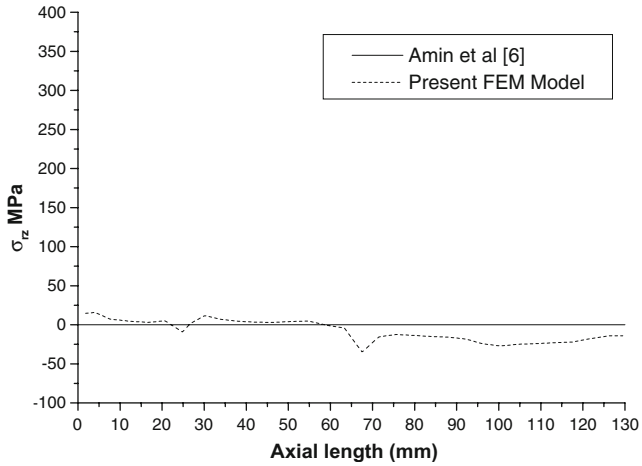

Fig. 8 Variation of shear stress (σ_{rz}) along the axial length

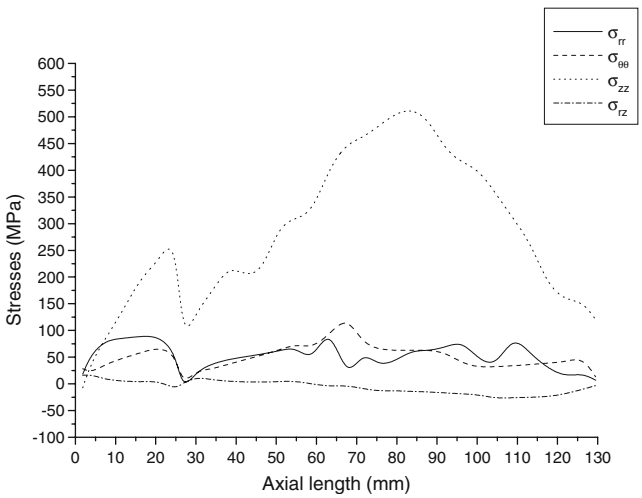

Fig. 9 Components of stresses along axial length at r=0.4047 mm

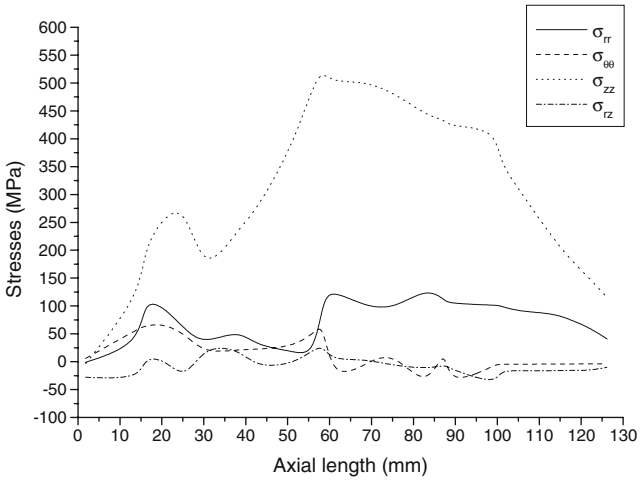

Fig. 10 Components of stresses along axial length at r=5 mm

$$[M]^e = \text{Elemental Mass matrix} = \int_D \rho[N]^{eT}[N]^e \ddot{u}.rdrdz$$

$$\{f_b\}^e = \text{Centrifugal Body force vector due to rotation} = \int_{B_q} [N]^{eT} \rho n^2 r.dB_q$$

$$\{f_t\}^e = \text{Traction force vector due to magnetostriction effect} = \int_{B_q} [N]^{eT} t_z dB_q$$

$$\{\sigma\}^e = \begin{Bmatrix} \sigma_{rr} \\ \sigma_{\theta\theta} \\ \sigma_{zz} \\ \sigma_{rz} \end{Bmatrix} \tag{6}$$

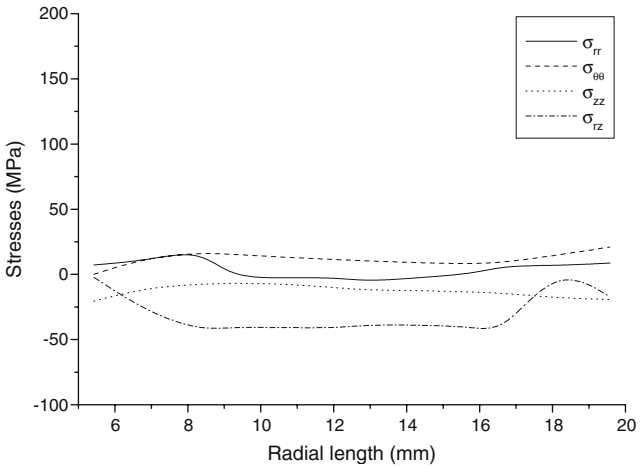

Fig. 11 Components of stresses along axial length at z=0.4047 mm

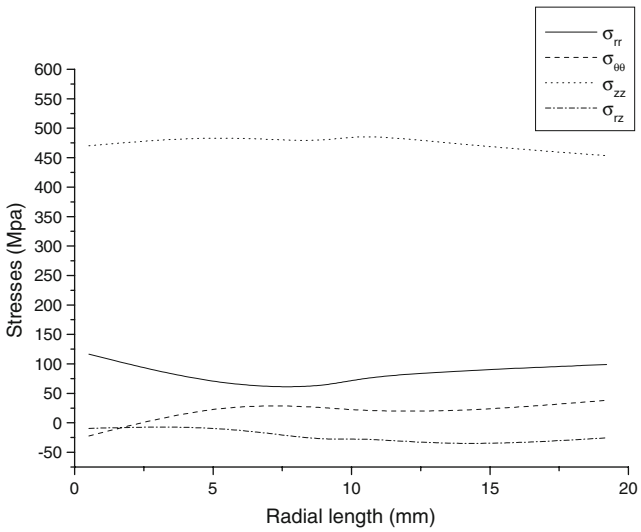

Fig. 12 Stress components along radius at z=45

The Gauss quadrature technique is used to evaluate elemental matrices, and the arrays are assembled as soon as they are computed. Quadrature formulae for integrals defined over a rectangular master element are derived from one-dimensional quadrature formulae as follows:

$$\begin{aligned} \int F(\xi,\eta)d\xi d\eta &= \int_{-1}^{1}\left[\int_{-1}^{1} F(\xi,\eta)d\eta\right]d\xi \\ &\approx \int_{-1}^{1}\left[\sum_{j=1}^{n} F\left(\xi,\eta_j\right)w_j\right]d\xi \\ &\approx \sum_{i=1}^{m}\sum_{j=1}^{n} F\left(\xi_i,\eta_j\right)\cdot w_i w_j \end{aligned} \tag{7}$$

where m and n denotes the number of quadrature points in ξ and η direction, ξ_i and η_i denotes the Gauss points, w_i and w_j denotes corresponding Gauss weight.

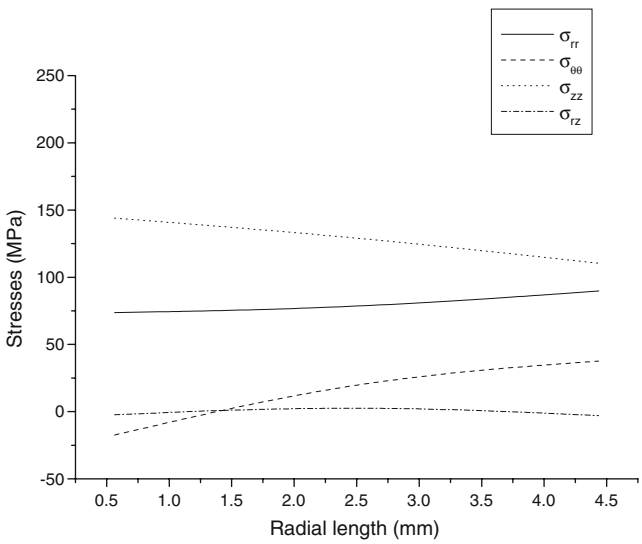

Fig. 13 Stress components on along radius at z=13 0 mm

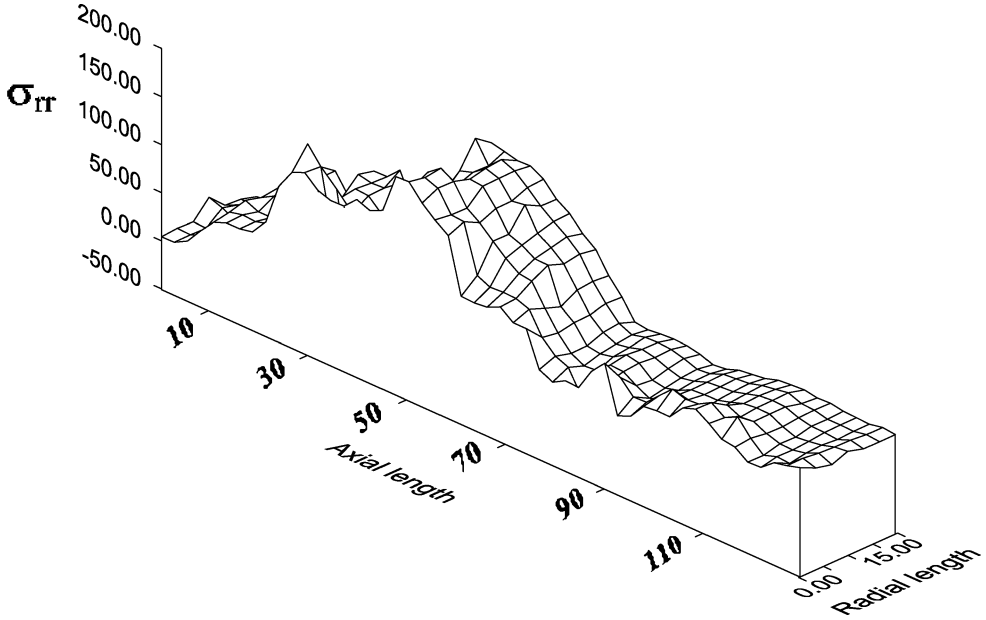

Fig. 14 3D stress surface plot for radial stress (σ_{rr})

3.1 Assembly

The assembly of elements is based on the idea that the solution and possibly its derivative of higher order equations are continuous at interelement boundaries.

$$\left([GK]_{nnm\times nnm} - \omega^2[GM]_{nnm\times nnm}\right)\{u\}_{nnm\times 1} = \{GF\}_{nnm\times 1} \tag{8}$$

where

$$\begin{aligned}
[GK]_{nnm\times nnm} &= \sum_{e=1}^{nem} [K]^e_{nne\times nne} \\
[GM]_{nnm\times nnm} &= \sum_{e=1}^{nem} [M]^e_{nne\times nne} \\
\{GF\}_{nnm\times 1} &= \sum_{e=1}^{nem} \{f\}^e_{nnb\times 1}
\end{aligned} \tag{9}$$

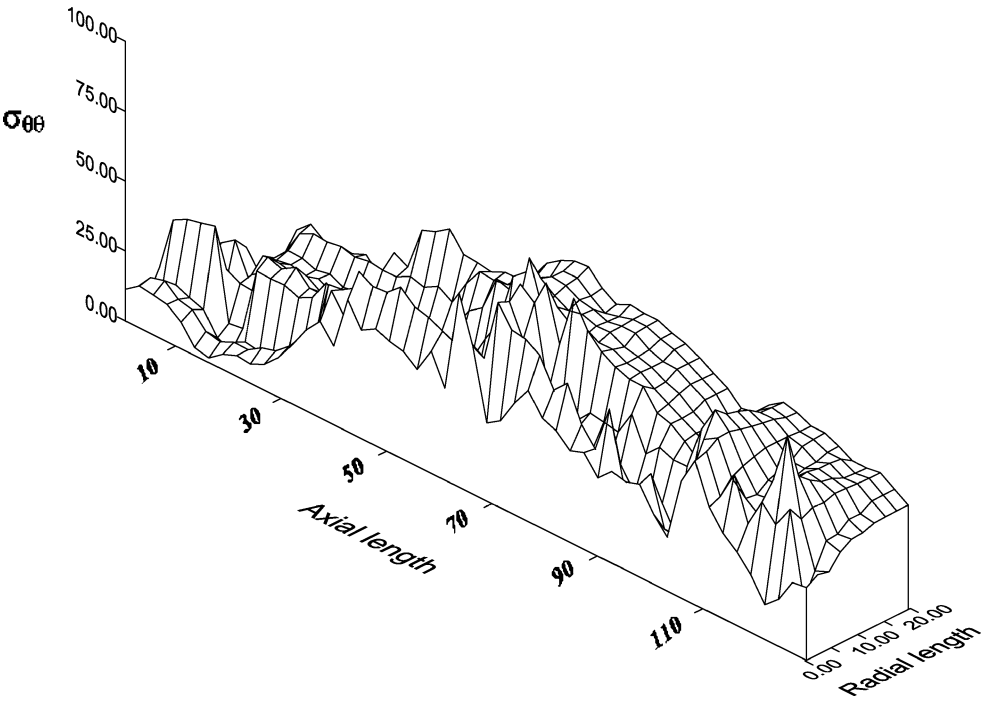

Fig. 15 3D stress surface plot for circumferential stress ($\sigma_{\theta\theta}$)

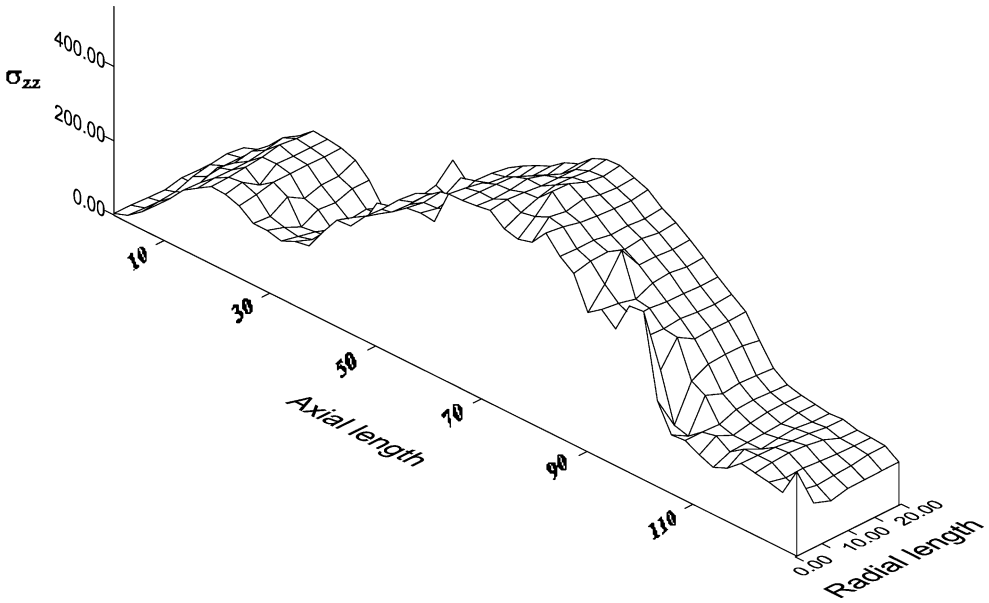

Fig. 16 3D stress surface plot for axial stress (σ_{zz})

3.2 Application of essential boundary conditions

The fifth and last step of formulation is to impose the actual boundary conditions. It is here that we require the weight function w to vanish at boundary points where the essential boundary conditions are specified.

The final equation we get has modified global

$$\left(\left[\widehat{K}\right]_{nnm\times 2\times nnm\times 2} - \omega^2\left[\widehat{M}\right]_{nnm\times 2\times nnm\times 2}\right)\{u\}_{nnm\times 2\times 1} = \left\{\widehat{F}\right\}_{nnm\times 2\times 1} \tag{10}$$

where, $\left[\widehat{K}\right]$ is modified global stiffness matrix, $\left[\widehat{M}\right]$ is modified global mass matrix, *{u}* is the nodal displacement vector and $\left\{\widehat{F}\right\}$ is modified global right side force vector.

3.3 Stress calculations

The strain-displacement relationship is given as [10, 11]

$$\{\varepsilon\} = \begin{Bmatrix} \varepsilon_{rr} \\ \varepsilon_{\theta\theta} \\ \varepsilon_{zz} \\ \varepsilon_{rz} \end{Bmatrix} = \begin{Bmatrix} \frac{\partial u}{\partial r} \\ \frac{u}{r} \\ \frac{\partial v}{\partial z} \\ \frac{\partial u}{\partial z} + \frac{\partial v}{\partial r} \end{Bmatrix} = [B]\{u\} \tag{11}$$

The stress-strain relationship is given by [10, 11]

$$\{\sigma\} = [D]\{\varepsilon\} \tag{12}$$

where stress vector,

$$\{\sigma\} = \{\,\sigma_{rr} \quad \sigma_{\theta\theta} \quad \sigma_{zz} \quad \sigma_{rz}\,\}^T$$

$\{\varepsilon\}$ is the strain vector, *[B]* is the matrix of nodal coordinates, *{u}* is the displacement vector, $\{\sigma\}$ is the

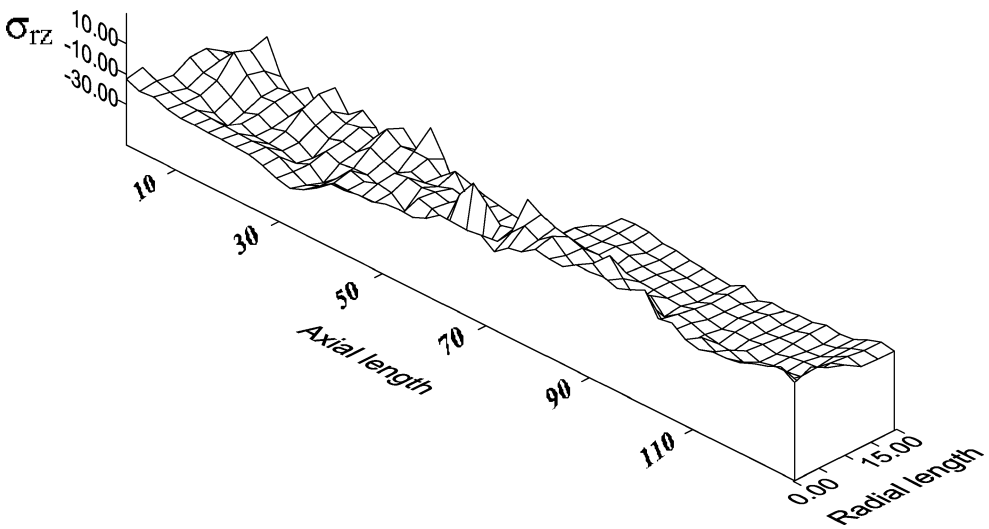

Fig. 17 3D stress surface plot for shear stress (σ_{rz})

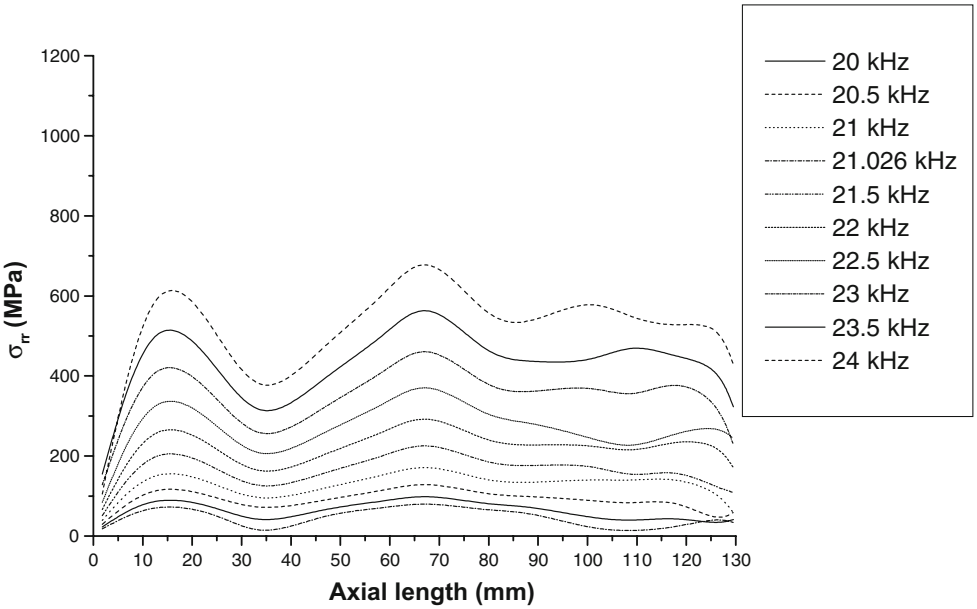

Fig 18 Effect of frequencies on σ_{rr}

stress vector and *[D]* is the matrix of the material elastic constants.

4 Results and discussion

In the present work, software has been developed using MATLAB for the calculation of natural frequency, displacement, and the stress components. For the use of this software, IDEAS is used as a preprocessor for the meshing. MS ORIGIN and SURFER software are used to present the results in graphical form. The output obtained using present software, in the form of nodal displacements, is used as an input for stress calculation. First the developed code is validated by comparing the results with the results given in literature [18]. Then the natural frequency, displacement and stresses are calculated for the horn domain for rotary USM.

4.1 Convergence test

The conical horn has been discretized by eight noded serendipity elements in both the axial and radial directions. The number of elements in the domain is increased from 5–300 and the natural frequency for resonance condition is calculated. As the horn is axis-symmetric in nature, we are getting the number frequencies equal to double the number of nodes. These are the Eigen values ω_i. The lowest non-zero ω_i is called the fundamental vibrational frequency. The plot of the variation of these natural frequencies with the elements is shown in Fig. 3. When fewer elements are used, significant errors occur because of the inaccurate

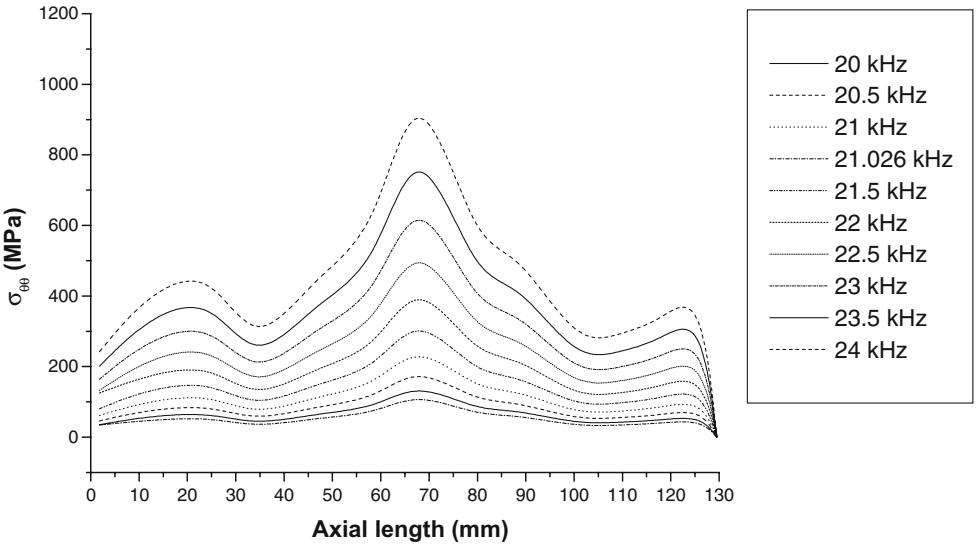

Fig 19 Effect of frequencies on $\sigma_{\theta\theta}$

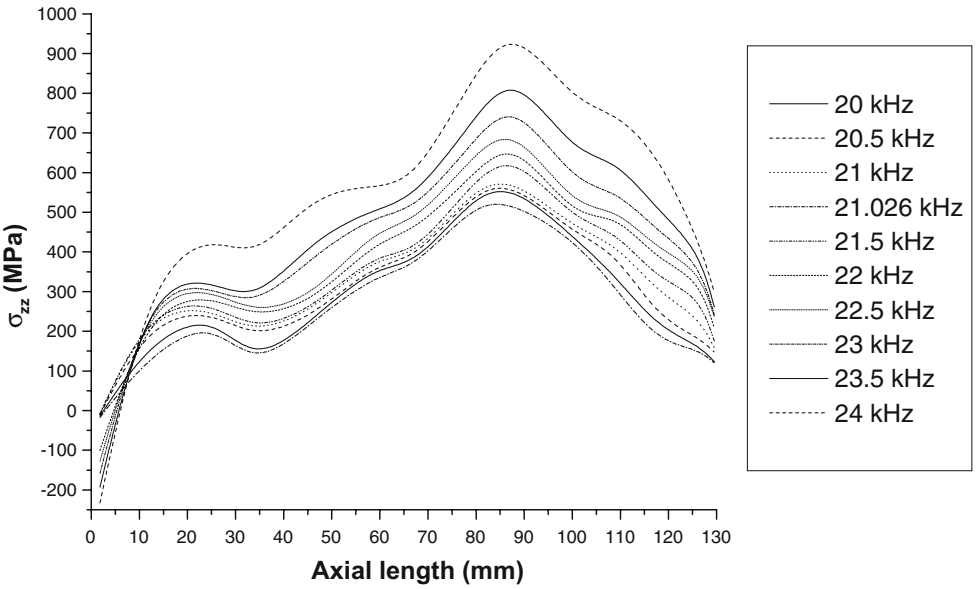

Fig 20 Effect of frequencies on σ_{zz}

approximation of the interpolation function to the actual solution within each element. With 100 or more elements there is no significant variation in the resonant frequency. So we choose to take 100 elements in the horn domain for further calculations.

4.2 Axial displacement of horn

The resulting displacements at the nodes provide the oscillations amplitude variation throughout the horn length as shown in Fig. 4. From this graph, the transducer displacement (15 μm) decreases to zero at the nodal point. Then the displacement changes direction and increases, reaching its maximum value at the nodal end. The end value for the given shape is 95 μm, which produces magnification factor of 6.3 [6].

4.3 Comparison

Relating the displacement to strains and stresses, the horn stresses can be obtained. Radial (σ_{rr}), circumferential ($\sigma_{\theta\theta}$), axial (σ_{rr}) and shear (σ_{rz}) stresses along the double conical horn length for the conventional USM are shown in Figs. 5, 6, 7, and 8, respectively. From these, in Fig. 6 it is shown that the stresses obtained by the present software and the stresses given in the literature are very close to each other. The error in this comparison is about 2% (see Table 1 for specifications).

The axial length of the horn is plotted against the circumferential stress ($\sigma_{\theta\theta}$), the curve obtained is similar to the curve given in [6] as shown in Fig. 6. This indicates the accuracy of the developed software. The error in these two plots is about 3%. The axial length of the horn is plotted

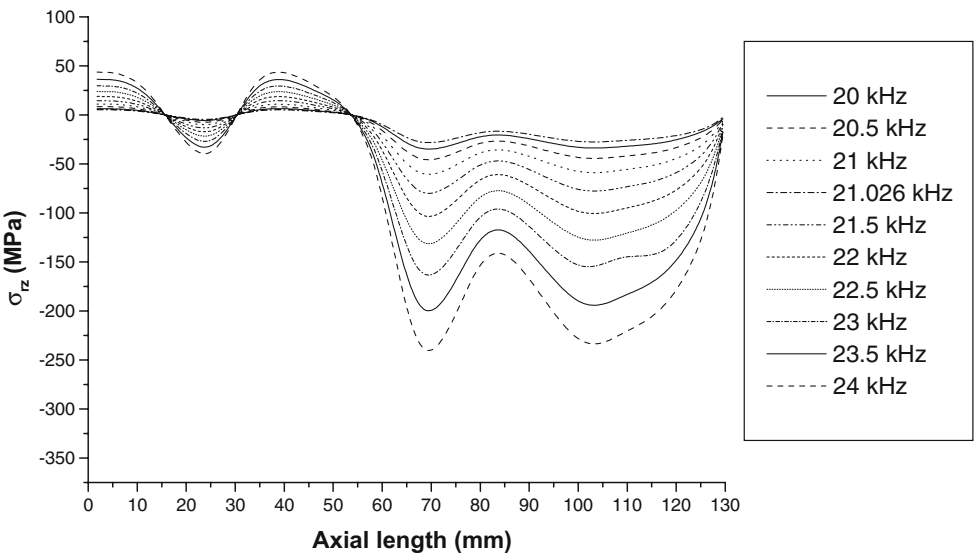

Fig 21 Effect of frequencies on σ_{rz}

against the axial stress (σ_{rr}), the curve obtained is similar to the curve given in [6] as shown in Fig. 7. This indicates the accuracy of the developed software. The error in these two plots is about 4%. The axial length of the horn is plotted against the shear stress (σ_{rz}) and the curve obtained is similar to the curve given in [6] as shown in Fig. 8. This indicates the accuracy of the developed software. The error in these two plots is about 1.5%.

4.4 Stresses in the horn with rotation

The displacement obtained for the rotary horn is related to the stress components. The variation of components of stresses along the z-axis at r=0.4047 mm is shown in Fig. 9. This figure indicates that the axial stress is the maximum stress, and it is responsible for a major part of the stresses developed in the horn domain while the other three stress components approach zero values over most of the horn length. The components of stresses starts with zero value at the transducer end and rises to a first peak due to stress concentration at the hole tip. The second higher peak value is obtained at the middle portion of the horn where the sudden change in the area of the horn domain occurs. The peak effective stress value for the horn at 250 rpm is about 500 MPa, which is below the allowable limit.

The variation of stress components along the axis at a radius of 5 mm is plotted in Fig. 10. Here it is observed that the axial stress is well below the allowable endurance strength of the horn material. The maximum peak value of axial stress is about 510 MPa, which is just below the maximum allowable endurance strength of the horn material. The variation of stress components along radius at axial length equal to 0 mm is plotted The stress distribution along the radial length is linear and it is nearly zero value at the transducer end as shown in Fig. 11.

Figure 12 shows the variation of stress components along radius at z=45 mm. The maximum axial stress is obtained in this region, as there is sudden change in the area. The maximum stress value in this area is 500 MPa, which is below the allowable endurance strength (520 MPa) of the horn material. It is also shown that the nature of the curve is linear along radius at a section where z=45 mm. The variation of stress components along radius at axial length equal to 130 mm is plotted. As the tool end of the horn is free to move, stress is decreased, and it approaches zero for the circumferential and shear stress as shown in Fig. 13, the 3D stress surface plot for the stress distribution over the whole horn length. It is plotted by taking radial length as a X-axis, axial length as a Y-axis and the stress component on the Z-axis. The 3D stress surface plot is created using SURFER software. The 3D stress surface plot for the radial stress (σ_{rr}) is shown in Fig. 14. From this figure it is shown that the stress distribution is nearly zero at the transducer end and it is maximum where the sudden change in the horn area occurs at the middle of the horn. The maximum (σ_{rr}) obtained at the middle of the horn by the present FEM model is well below the maximum allowable stress.

Figure 15 shows the 3D stress surface plot for the domain and the circumferential stress ($\sigma_{\theta\theta}$). The maximum stress obtained at the critical area of the horn is also well below the allowable stress. Figure 16 shows the 3D stress

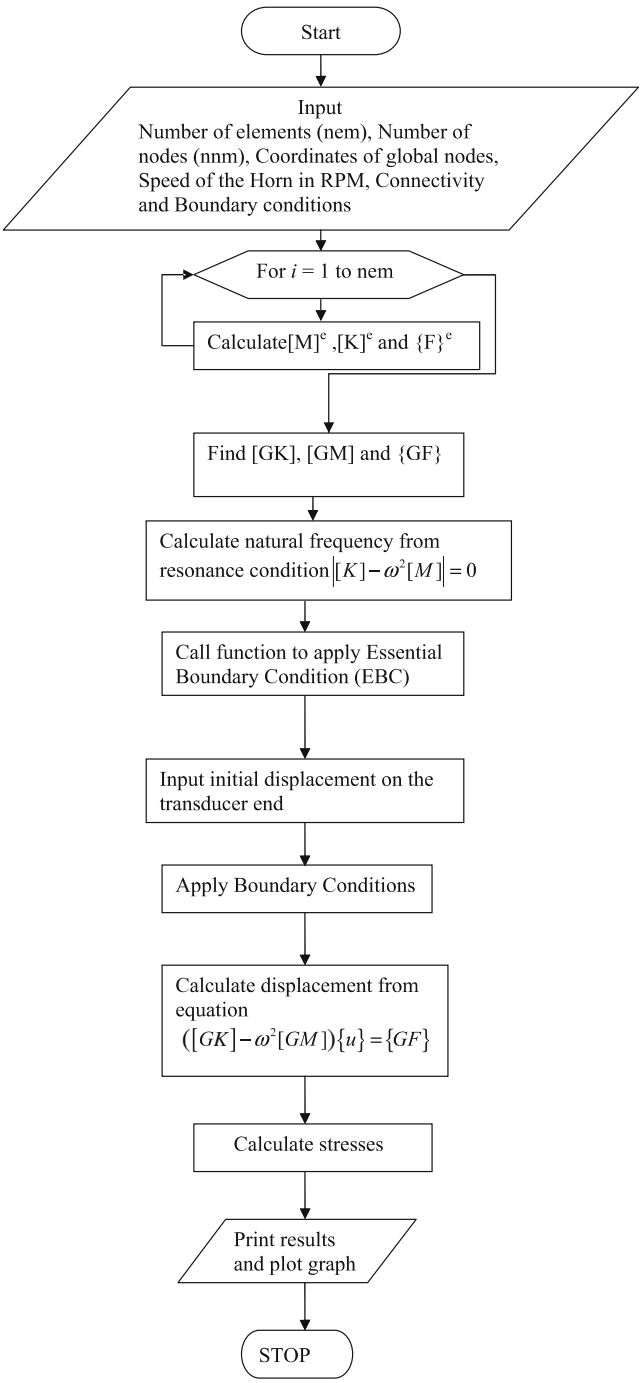

Fig 22 Flow chart for calculation of stresses

surface plot between the radial length, axial length and the axial stress (σ_{zz}). For the double conical horn of rotary USM, the maximum axial stress of 500 MPa is obtained where the abrupt change in the area occurs and reduces further near the tool end. The axial stress is nearly zero at the transducer end and the first peak value is obtained of about 200 MPa because of the hole.

Figure 17 shows the 3D stress surface plot between radial length, axial length and the shear stress (σ_{rz}). The shear stress obtained for the double conical horn is nearly zero over the whole domain. Figures 18, 19, 20, and 21 show the plots between axial length of the horn and the components of stresses for the various frequencies. These figures show that as the frequency increases, the stress variation over the horn domain increases, but at the resonance frequency (21.026 kHz), the stress is much less compared to the stresses for other frequencies.

Figure 22 shows flow chart for calculation of stresses.

5 Conclusions

This work has covered the design of a horn for rotary ultrasonic machining using the finite element method. The amplitude of vibration and the stress components induced within the horn domain are calculated and the conclusions of the present work are as follows:

- A mathematical model for the determination of displacement within the horn used in rotary ultrasonic machining is developed. The components of stresses within the horn domain are found to be within the allowable stress.
- The amplification factor is more for rotary USM over conventional USM without horn rotation for the same material properties and the boundary conditions.
- The first peak value for the stress components are obtained near the top of the horn because of the hole concentration in that region.
- The maximum stresses are obtained at the middle surface of the horn where the area changes suddenly but it is well within the maximum allowable stress for the horn material.
- The stresses at the bottom surface of the horn are nearly zero because the horn is free to move at that end.
- The stress components are linear over the radial length of the horn.
- The stresses obtained for the resonance frequency is much less than the stresses obtained for the other frequencies.

References

1. Rozenberg LD, Kazantsev VF, Markov IA, Yakhinov DF (1964) Ultrasonic cutting. Consultancy Bureau, New York
2. Ghosh A, Mallik AK (2002) Manufacturing science. EWP Publications, New Delhi (INDIA)
3. Kremer D, Ghabrial SM, Moisan A (1981) The state of the art of ultrasonic machining. Ann CIRP 30:107–110
4. Ya G, Qin HW, Yang SG, Xu YW (2002) Analysis of the rotary machining mechanism. J Mater Process Technol 129:182–185
5. Gilmore R (1991) Ultrasonic machining: a case study. J Mater Process Technol 28:139–148
6. Amin SG, Ahmed MHM, Youssef HA (1995) Computer-aided design of acoustic horns for ultrasonic machining using finite element analysis. J Mater Process Technol 55:254–260
7. Seah KHW, Wong YS, Lee LC (1993) Design of tool holders for ultrasonic machining using finite element method. J Mater Process Technol 37(1.4):801–816
8. Komaraiah M, Narasimha Reddy P (1991) Rotary ultrasonic machining—a new cutting process and its performance. Int J Prod Res 29(11):2177–2187
9. Komarajah M, Reddy PN (1990) Role of tool materials in USM. Proc 14th AIMTDR Conference, IIT, Bombay, India
10. Pei ZJ, Ferreira PM (1999) An experimental investigation of rotary ultrasonic face milling. Int J Mach Tool Manuf 39: 1327–1344
11. Thoe TB, Aspinwall DK, Wise MLH (1998) Review of ultrasonic machining. Int J Mach Tool Manuf 38(4):239–255
12. Timoshenko SP, Goodier JN (1970) Theory of elasticity. McGraw-Hill International Edition, Singapore
13. Timoshenko SP, Weaver W, Young DH (1990) Vibration problems in engineering. Wiley, Singapore
14. Satyanarayana A, Krishna Reddy BG (1984) Design of velocity transformers for ultrasonic machining. Electr India 24:11–20
15. Rao SS (2001) The finite element methods in engineering. Butterworth-Heinmann, Delhi
16. Reddy JN (2005) An introduction to finite element method. McGraw-Hill Company, Singapore
17. Kwon YW, Bang H (2000) The finite element method using MATLAB. CRC Press, Boca Raton, FL
18. Yadava V, Jain VK, Dixit PM (2002) Thermal stresses due to electric discharge machining. Int J Mach Tools Manuf 42(8): 877–888